ELSEVIER

Contents lists available at ScienceDirect

Journal of Non-Crystalline Solids

journal homepage: www.elsevier.com/locate/jnoncrysol





New interaction potentials for alkaline earth silicate and borate glasses

Yueh-Ting Shih^a, Siddharth Sundararaman^b, Simona Ispas^c, Liping Huang^{a,*}

- ^a Department of Materials Science and Engineering, Rensselaer Polytechnic Institute, Troy, NY 12180, United States
- b Lawrence Berkeley National Laboratory, Berkeley, CA 94720, United States
- ^c Laboratoire Charles Coulomb (L2C), University of Montpellier, CNRS, Montpellier, France

ARTICLE INFO

Keywords: Molecular dynamics simulation Interaction potential Alkaline earth silicate Alkaline earth borate Structure Elastic properties

ABSTRACT

New interaction potentials were developed for molecular dynamics simulations to study the role of Mg and Ca in modifying the structure and properties of alkaline earth silicates and borates. Competition between the depolymerization of the silica network and the formation of new bonds between oxygen atoms and modifiers leads to the enhancement of the elastic moduli with increasing modifier content in alkaline earth silicate glasses. Compared with calcium silicate, the higher elastic moduli of magnesium silicate result from a higher connectivity of the overall glass network due to the incorporation of fourfold coordinated magnesium and a more rigid connection between oxygen atoms and modifiers. In contrast to the silicates, the effect of modifier on the elastic moduli of alkaline earth borates is dominated by the formation of fourfold coordinated boron (N_4) . Calcium borate with higher N_4 shows a more rigid network structure and higher elastic moduli.

1. Introduction

Calcium silicates are commonly found in bioactive materials for medical treatment and cementitious materials for construction [1-5]. Previous studies indicated that substitution of CaO by MgO in silicate glasses modifies their chemical durability and increases the fracture toughness with a concomitant decrease of the Young's modulus [6–10]. The unique properties of magnesium-containing glass may be attributed to the distinctive role of magnesium in the glass network. Based on the classical glass formation theory [11], when added into the glass network, alkaline earth ions act as network modifiers to break the connectivity of the network and form non-bridging oxygens (NBOs). However, as magnesium is known to have a high field strength and a high electronegativity, its bond with oxygen exhibits some covalent characters and thus it behaves more like a network former, as shown in several experimental and simulation studies [8-10,12-22]. From the infrared (IR) spectra of aluminosilicate glasses, the calculated ionicity is 0.9 for calcium but only 0.7 for magnesium, which explains the covalent character of magnesium-oxygen bonds [12]. The deconvolution of ²⁹Si nuclear magnetic resonance (NMR) spectra of silicate-based bioactive glasses with the composition of 49.5SiO₂-1.1P₂O₅-23.0((1- x) CaO-xMgO)-26.4Na₂O suggests that, although 86% of the magnesium oxide acts traditionally as a network modifier, up to 14% of the magnesium oxide enters the glass network as MgO4 tetrahedron, resulting in

an increased polymerization of the glass network [9]. Similarly, previous molecular dynamics (MD) simulations of substitution of CaO with MgO in soda-lime silicate and silicate-based bioactive glasses showed that the higher field strength of Mg leads to a different structure compared to the effect of Ca [8,10]. More specifically, Ca ions, coordinated by six oxygen atoms, act as network modifier, while some of the Mg ions are coordinated by four oxygen atoms to form MgO₄ tetrahedron and interconnect with the SiO₄ network.

For another important glass former, boron, the addition of MgO results in a unique structural change in the glass network as well. The fraction of fourfold coordinated boron (N_4) from NMR and FTIR results indicated a smaller amount of N_4 in magnesium borate compared with other alkaline earth borates at the same modifier content [23,24]. Although, several studies investigated the structure and properties of the magnesium-containing silicate and borate, most of them focused on a narrow composition range [8,10,24]. To systematically study the effect of MgO on structure and properties of silicate and borate melts and glasses in comparison with CaO, reliable interaction potentials are needed to model these systems over a large composition range and under different thermodynamic conditions. Two-body potentials based on the Buckingham functional form recently developed by Wang et al. [25] and by Deng et al. [26] are two promising candidates. By adding interaction parameters for boron to the Guillot and Sator potential [27], the Wang's potential shows a good agreement with experiments on structure and

E-mail address: huangL5@rpi.edu (L. Huang).

^{*} Corresponding author.

properties of borosilicate glasses and liquids. Furthermore, it has a high transferability with no composition-dependent parameters. Started from the pairwise potential developed by Kieu et al. [28], the Deng's potential well reproduced the structure and elastic moduli of borosilicate and boroaluminosilicate. However, similar to the Kieu potential, it has a composition dependent boron energy parameter that was fitted to the experimental boron coordination trends as a function of compositions. This makes it hard to transfer to the systems other than borosilicate glasses. Moreover, a benchmark work carried out recently by Lee et al. indicated that both the Wang's and Deng's potentials cannot accurately predict the elastic moduli of commercial borosilicate glasses Boro33 and N-BK7 due to the imprecise description of N_4 as a function of compositions [29].

Based on the Buckingham functional form, we recently used an optimization scheme similar to the one developed for silica glass [30] and extended the interaction parameter set to include alkali modifiers (Li, Na and K) and alkaline earth modifier (Ca), network former boron, and aluminum that can behave as a modifier or a former depending on the composition [31,32]. In this work, we adapted a similar optimization approach to develop interaction parameters for Mg-O, Mg-Si, Mg-Mg, Mg-B, and Ca-B pairs. One of the major goals of our potential optimization scheme is hence to not have any system specific parameters to ensure easy transferability and extensibility to complex multi-component systems. Reliable pairwise potentials will allow for high computational efficiency to study large and complex systems.

The article is organized as follows: first, the reliability of the potential for alkaline earth silicate will be demonstrated by comparing with the *ab initio* and experimental data. Second, the structure and properties of magnesium silicate will be discussed and compared with those of calcium silicate. Afterward, we will investigate the structure and properties of magnesium and calcium borates, and then compare them with those of silicates.

2. Simulations methods

In this section, we present the optimization procedure and the details about the generation of the glass samples for the investigation of composition-structure-properties relationship in alkaline earth silicates and borates.

2.1. Potential and cost function

As for our previous studies [30–32], we used the Buckingham potential functional form for the short-range interactions and the Wolf truncation method to evaluate the Coulombic interactions [33–35].

$$V^{Buck}(r_{\alpha\beta}) = A_{\alpha\beta}exp(-B_{\alpha\beta}r_{\alpha\beta}) - \frac{C_{\alpha\beta}}{r_{\alpha\beta}^6} + \frac{D_{\alpha\beta}}{r_{\alpha\beta}^4} + V^W(r_{\alpha\beta})$$
 (1)

where

$$V^{W}(r_{\alpha\beta}) = q_{\alpha}q_{\beta} \left[\frac{1}{r_{\alpha\beta}} - \frac{1}{r_{cut}^{W}} + \frac{(r_{\alpha\beta} - r_{cut}^{W})}{(r_{cut}^{W})^{2}} \right]$$
 (2)

and $\alpha, \beta \in \{O, Si, B, Mg, Ca\}$. All the parameters from our previous studies [30–32] were maintained constant and oxygen charge (q_O) was evaluated for each composition in order to maintain the charge neutrality [36]. For instance:

$$q_O = \frac{xq_{Mg} + 2(1 - x)q_B}{2x - 3} \tag{3}$$

which is for magnesium borate with the composition of xMgO–(1-x) B_2O_3 , where q_{Mg} and q_B are the charge of magnesium and boron, respectively.

The short-range interactions were cut off at 8 Å while the Coulombic interactions were cut off at 10 Å for the Wolf method, same as those used

Table 1Number of atoms and density used to equilibrate liquid at high temperatures in *ab initio* MD simulations.

System	N (atoms)	ρ (g/cm ³)
$0.5 \text{MgO-} 0.5 \text{SiO}_2$	400	2.75
0.4 CaO -0.6 SiO $_2$	390	2.78
$0.5MgO-0.5B_2O_3$	392	2.36
0.5 CaO -0.5 B $_2$ O $_3$	392	2.50

in our previous studies [30–32]. MD simulations were carried out using the LAMMPS [37] (Large-scale Atomic/Molecular Massively Parallel Simulator) with a timestep of 1.6 fs. A smaller timestep of 0.8 fs was used during the optimization process when exploring the parameter space to avoid large temporary forces that might arise.

The cost function for optimizing the parameters follows our scheme in previous work [30-32] and is given by

$$\chi^{2}(\phi) = w_{1} \int_{0}^{r_{N_{RDF}}} \sum_{\alpha,\beta} \left(rg_{\alpha\beta}^{calc,T}(r|\phi) - rg_{\alpha\beta}^{ref,T}(r) \right)^{2} dr + w_{2} \left(E^{calc,300K}(\phi) - E^{ref,300K} \right)^{2} + w_{3} \left(\rho^{calc,300K}(\phi) - \rho^{ref,300K} \right)^{2} + w_{4} \left(C^{calc,300K}(\phi) - C^{ref,300K} \right)^{2}$$

$$(4)$$

where ϕ is the current parameter set, α, β are the different species, w_1 , w_2 , w_3 , w_4 are the weights for each contribution, $rg_{\alpha\beta}(r)$ is the radial distribution function (RDF) weighted by the distance r up to a maximum distance of $r_{N_{RDF}} = 7$ Å at temperature T = 3500 K and 3000 K for silicate and borate, respectively. E is the Young's modulus, ρ is the density and C is the average boron coordination at 300 K and ambient pressure, which is only included in the optimization of potential parameters for borates. The superscript "ref" refers to the first principles or experimental reference data towards which the optimization was carried out, and the superscript "calc" refers to the calculated properties using the current parameter set. It should be noted that there is no experimental data available for the Young's modulus of magnesium borate, thus its cost function only includes RDF, density, and the average boron coordination number. The composition of 0.5MgO-0.5SiO2, 0.4CaO-0.6SiO2, 0.5MgO-0.5B₂O₃ and 0.5CaO-0.5B₂O₃ were used for each glass system in the potential optimization process.

The RDFs for "calc" were calculated by equilibrating a sample of 1200 atoms and 1500 atoms for magnesium silicate and calcium silicate at 3500 K, respectively, 1400 atoms for magnesium and calcium borate at 3000 K with the density given in Table 1. Samples were first equilibrated for 30 ps in the canonical (NVT) ensemble, and configurations from the next 40 ps were used to calculate RDFs.

Density and average boron coordination at room temperature were measured during the optimization process by relaxing the quenched samples of $\sim\!10000$ atoms in the NPT ensemble at 300 K and ambient pressure with the current parameter set. The Young's modulus was then measured by compressing and expanding the samples at 300 K along one direction at a constant strain rate (1.25 ns $^{-1}$) up to a linear change of 0.6% and measuring the stress response:

$$E_{x} = \frac{d\sigma_{x}}{d\varepsilon_{x}} \tag{5}$$

where E_x , σ_x and ε_x are the Young's modulus, stress, and strain, respectively, along the x-direction.

Minimization of the cost function was performed using the

Table 2Charge for different species.

Species	Si	В	Ca	Mg
Charge (e)	1.7755	1.6126	1.4977	1.085

Table 3 Short-range interaction parameters.

i-j	A _{ij} (eV)	B_{ij} (\mathring{A}^{-1})	C_{ij} (eV·Å 6)	$D_{ij}~(eV{\cdot}\mathring{A}^{24})$
0-0	1120.5	2.8927	26.132	16800
O-Si	23108	5.0979	139.70	66.0
Si-Si	2798.0	4.4073	0.0	3423204
O-Mg	139373	6.0395	79.562	16800
Si-Mg	516227	5.3958	0.0	16800
Mg-Mg	19669	4.0000	0.0	16800
O-Ca	146905	5.6094	45.073	16800
Si-Ca	77366	5.0770	0.0	16800
Ca-Ca	21633	3.2562	0.0	16800
O-B	16182	5.6069	59.203	32.0
B-B	1805.5	3.8228	69.174	6000.0
Mg-B	5000.0	4.0533	0.736	16800
Ca-B	848.55	5.9826	81.355	16800

 Table 4

 Compositions of glass systems studied in this work.

Composition
$\begin{array}{l} \text{xMO-}(1\text{-x})\text{SiO}_2\\ (M \in Mg; x \in 0, \ 0.1, \ 0.2, \ 0.3, 0.4, \ 0.5, \ 0.66)\\ (M \in Ca; x \in 0, \ 0.1, \ 0.2, \ 0.3, \ 0.4, \ 0.5) \end{array}$
$\begin{split} &x\text{MO-}(1\text{-}x)B_2\text{O}_3\\ &(\textit{M} \in \textit{Mg},\textit{Ca};x \in 0,\ 0.1,\ 0.2,\ 0.3,\ 0.4,\ 0.5) \end{split}$

Levenberg-Marquardt algorithm [38,39] and the numerical derivatives were calculated using a finite difference method. More detail about the optimization scheme can be found in our previous studies [30-32].

Partial charges and short-range interaction parameters used in this study, including the newly optimized charge of Mg, interaction parameters of Mg-O, Mg-Si, Mg-Mg, Mg-B, and Ca-B pairs, are given in Table 2 and Table 3, respectively. The new potentials will be referred to as "SHIK" (Sundararaman, Huang, Ispas, Kob) in the rest of the paper, following our previous studies [30–32].

2.2. Generation of ab initio reference data

The Vienna ab initio package (VASP) was used to perform the *ab initio* MD simulations [40,41]. The Kohn–Sham (KS) formulation of the density functional theory with generalized gradient approximation (GGA) and the PBEsol (modified Perdew-Burke-Ernzerhof) functional was used to describe the electronic structure [42–44]. The projector-augmented-wave formalism was used for the electron-ion interaction for Kohn-sham orbitals expanded in the plane wave basis set at the Γ point of the supercell with energies up to 600 eV [45,46]. The electronic convergence criterion for the residual minimization method-direct inversion in iterative space was fixed at 5×10^{-7} eV. These parameters were chosen based on previous studies performed on various silicate and borosilicate melts and glasses [30–32,47,48].

Ab initio MD simulations were carried out in the NVT ensemble at 3500 K and 3000 K for silicates and borates, respectively, using the Nosé thermostat to control the temperature [49]. To save some computational cost, the initial configurations for ab initio MD simulations were obtained by using the Pedone potential [50] for silicates at 3500 K and Wang's potential [25] for borates at 3000 K, respectively, in classical MD simulations. A cubic system of N atoms with periodic boundary conditions was used with the simulation box length fixed to a value corresponding to an experimental density under ambient conditions for each composition (see details in Table 1) [51–55]. For borates, a density of about 10% less than experimental glass density was chosen in order to reduce the pressure for faster diffusion during the equilibration of liquid at high temperature. The ab initio MD simulation for a given composition was

stopped once the mean squared displacement of the slowest element, i. e., silicon/boron, reached $\sim\!10~\text{Å}^2$, which was sufficient for other species to reach the diffusive regime too. We discarded the first 1 to 2.5 ps of the trajectory in each case and used the remaining data for calculating the reference RDFs for the potential fitting and for other structural properties presented in Sections 3.1 and 3.3.

2.3. Generation of MD simulation samples

Glasses of various compositions, as shown in Table 4 were prepared using the melt-quench method. Samples with ~ 10000 atoms were first equilibrated in the NVT ensemble for about 100 ps at about the experimental glass density at 3500 K and 3000 K for silicate and borate, respectively, and then in the NPT ensemble for about 500 ps at 0.1 GPa. They were then subsequently quenched to 300 K in the NPT ensemble at a nominal quench rate of ~ 1 K/ps. The small pressure of 0.1 GPa was applied at high temperature as a precaution to present the system from entering the gas phase, which was ramped down to 0 GPa during the quenching process. The samples were then annealed at 300 K and 0 GPa for 100 ps in the NPT ensemble. Four independent samples were quenched for each composition to improve the statistics of the results. To investigate the pressure effect on glass, the sample was compressed/ decompressed at a rate of 0.2 GPa/ps in the NPT ensemble. After every compression/decompression step, the sample was equilibrated for 90 ps, followed by another 10 ps to calculate the density.

3. Results and discussion

In this section, the reliability of the interaction potential for magnesium and calcium silicates will be shown in Section 3.1. The structure and properties of silicates will be discussed in the following Section 3.2. Afterward, the reliability of the interaction potential for magnesium and calcium borates, and the structure and properties of borates will be discussed in Sections 3.3 and 3.4, respectively.

3.1. Structure of magnesium and calcium silicate liquids

Fig. 1 shows partial RDFs of $0.5 \text{MgO} - 0.5 \text{SiO}_2$ and $0.4 \text{CaO} - 0.6 \text{SiO}_2$ liquids at 3500 K from classical MD by using the newly developed potential, in comparison with *ab initio* simulation results. The RDF data for calcium composition are extracted from our previous study [31]. Overall, the new potential well reproduces the structure of the melt as predicted by the *ab initio* simulations. This is not that surprising as RDFs were included in the cost function that was minimized. Meanwhile, it is important to note that the discrepancies observed in some of the RDFs are not entirely due to the shortcomings of the pair-wise potential functional form, as compromises in the optimization have to be made to predict different properties over a wide range of compositions [30,31].

Fig. 2 shows bond angle distributions (BADs) for the same two liquids as in Fig. 1. Although these BADs were not included in the cost function, overall a good agreement is seen between MD and *ab initio* data. The BAD of Si-O-Si and Si-Si-Si shift slightly to the left in both magnesium silicate and calcium silicate liquids, consistent with the shorter Si-Si distance in classical MD as seen in Fig. 1(d). This indicates a more rigid glass network structure in classical MD compared to that in *ab initio* simulation. Moreover, the BAD of Si-Si-Si exhibits a higher peak at 60 degrees, suggesting more 3-membered rings in the classical MD.

3.2. Structure and properties of magnesium and calcium silicate glasses

In this subsection, we will present a number of structural signatures and mechanical properties of magnesium and calcium silicates calculated from MD simulations and compare with existing experimental data to show the reliability of the new potential to describe them over a large composition range and under different thermodynamic conditions.

The Qⁿ species indicate the degree of polymerization of the silica

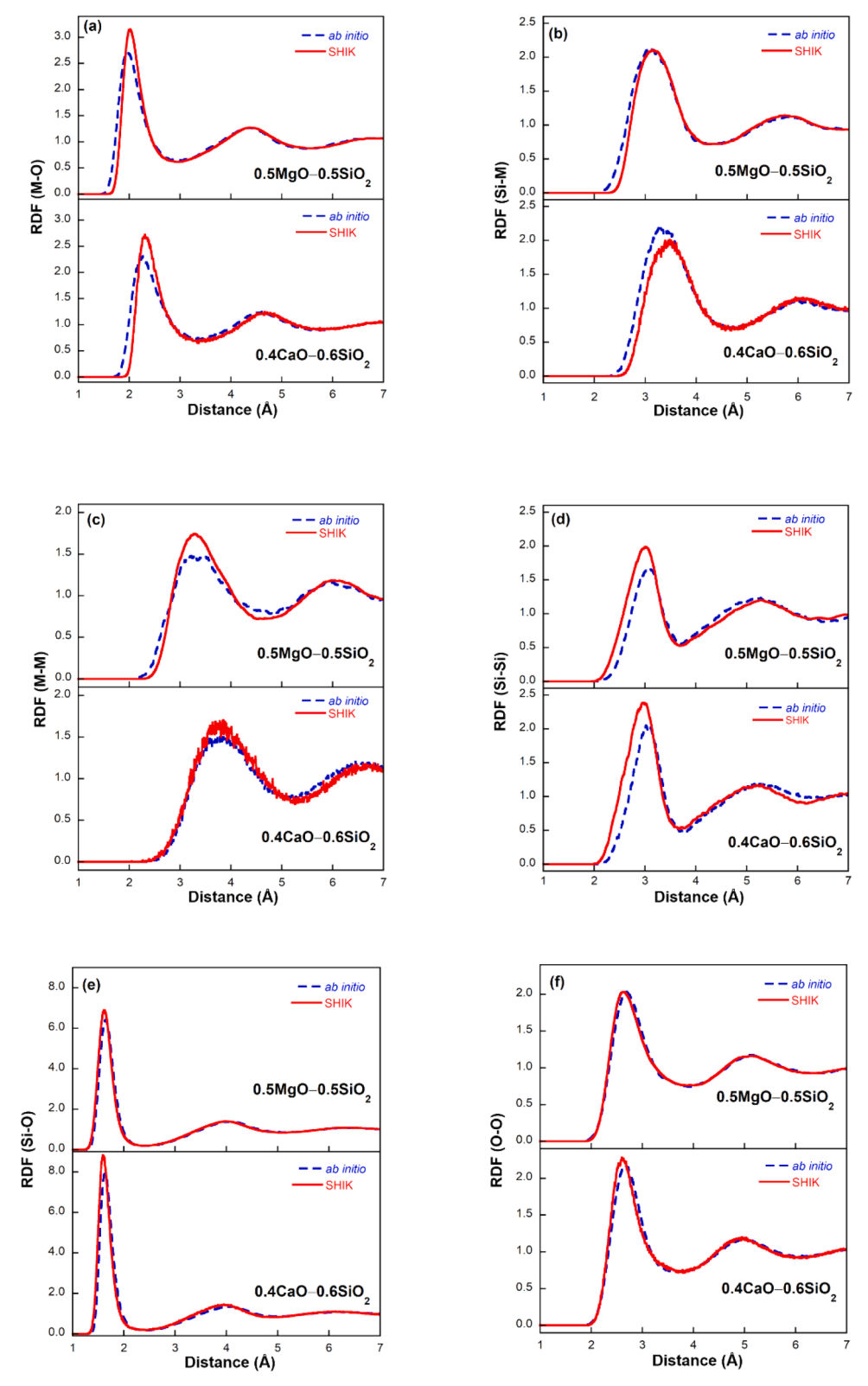


Fig. 1. Radial distribution functions (RDFs) of (a) M-O, (b) Si-M, (c) M-M (M = Mg or Ca), (d) Si-Si, (e) Si-O, and (f) O-O pair in 0.5MgO-0.5SiO₂ and 0.4CaO-0.6SiO₂ liquids obtained from the *ab initio* (blue dashed line) and the SHIK potential (red solid line) simulations at 3500 K.

network, where n is the number of bridging oxygen (BO) in the SiO₄ tetrahedron. As seen from the Q^n distribution in Fig. 3(a), the polymerization of the glass network is decreased with increasing modifier content. Moreover, magnesium silicate (solid symbol) exhibits a slightly higher degree of polymerization/connectivity than calcium silicate

(open symbol) at a given modifier content.

A similar trend is observed in the fraction of different oxygen species in Fig. 3(b), the BO decreases and NBO increases with the increasing modifier content. Magnesium silicate has a slightly higher fraction of BO and a lower fraction of NBO than calcium silicate at a given modifier

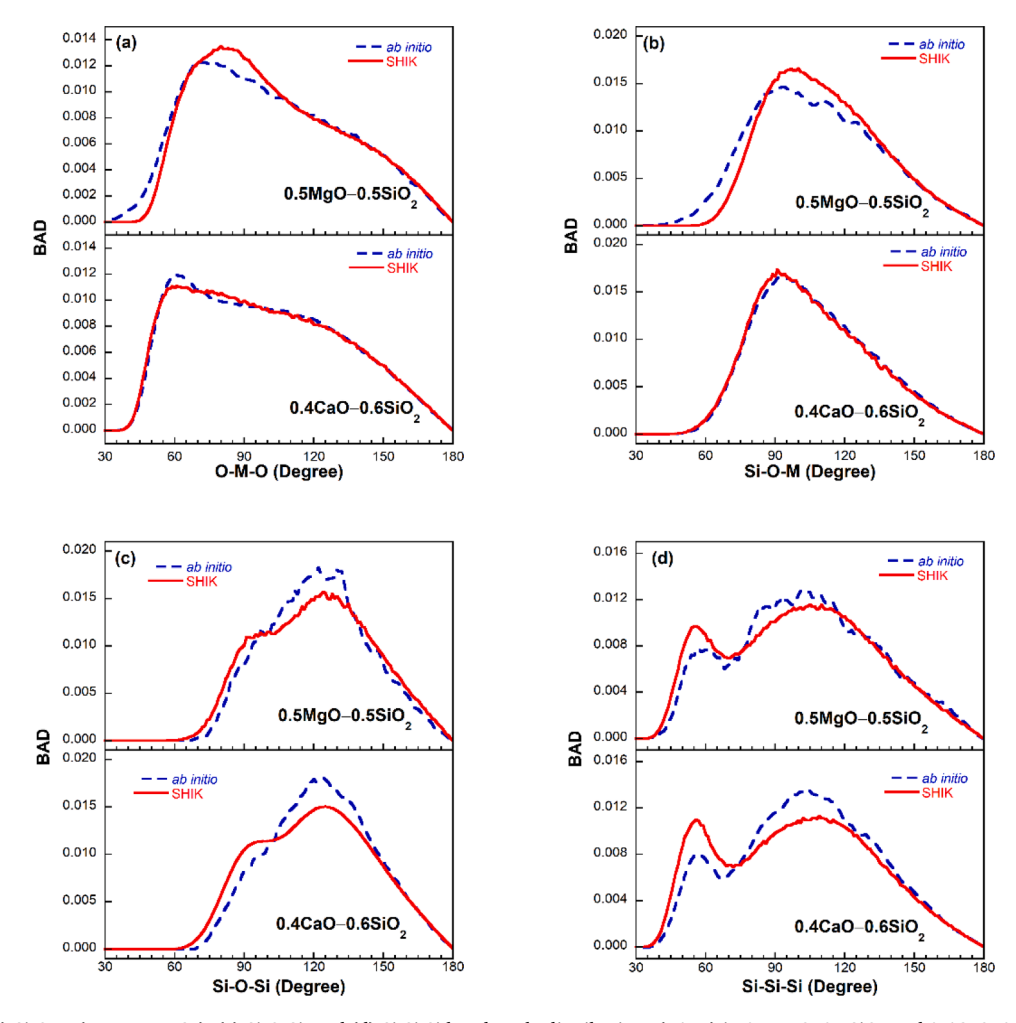


Fig. 2. (a) O-M-O, (b) Si-O-M (M= Mg or Ca), (c) Si-O-Si, and (d) Si-Si-Si bond angle distributions (BADs) in 0.5MgO-0.5SiO₂ and 0.4CaO-0.6SiO₂ liquids obtained from the *ab initio* (blue dashed line) and the SHIK potential (red solid line) simulations at 3500 K.

content, indicating a slightly higher degree of the polymerization in the glass network in the former than in the latter. In addition, free oxygen (FO), the oxygen not bonded to any silicon, but to modifier ions instead as seen in Fig. 3(c), increases with the increasing modifier content and has a slightly higher fraction in magnesium silicate than in calcium silicate at higher modifier content. This observation indicates that the high field strength of Mg can better stabilize the local negative charge and thus promote the formation of FOs and MgO4 tetrahedra, which are connected with the SiO4 tetrahedra and incorporated into the glass network.

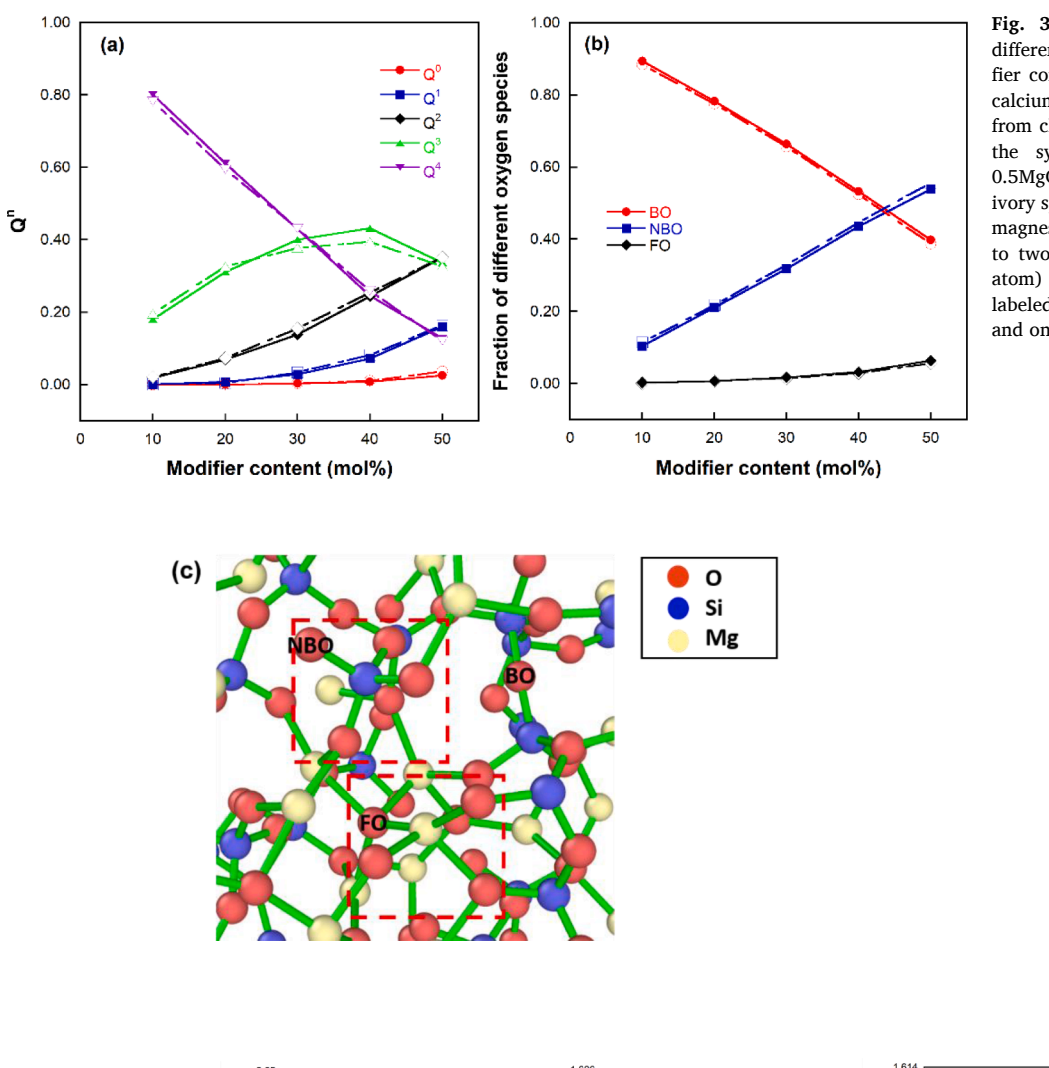
The average atomic distance inside SiO_4 tetrahedron as a function of modifier content in magnesium silicate and calcium silicate are shown in Fig. 4. At a given modifier content, calcium silicate exhibits shorter O-O, Si-BO, and Si-NBO distance than magnesium silicate. The O-O distance decreases with increasing modifier content in magnesium silicate and calcium silicate; whereas, magnesium silicate exhibits a smaller decreasing trend than calcium silicate. Similar to the O-O distance, both the Si-BO and Si-NBO distance decrease obviously with increasing modifier content in calcium silicate and exhibit insignificant change with increasing modifier content in magnesium silicate. This indicates that SiO_4 tetrahedra are less perturbed by the addition of modifiers in magnesium silicate than in calcium silicate.

Fig. 5 shows the atomic distance and inter-tetrahedral angle between SiO_4 tetrahedra, and the structural information between the modifier and SiO_4 tetrahedron. Larger inter-tetrahedral (Si-O-Si) angle, O-M-O

 $(M=Mg\ or\ Ca)$ and Si-O-M angle are observed in magnesium silicate than those in calcium silicate at a given modifier content. In contrast to the obvious decreasing trend of Si-O-Si and Si-O-M, the O-M-O exhibits a very small change with increasing modifier content. At a given modifier content, the Si-Si distance in magnesium silicate is longer than that in calcium silicate, whereas the opposite is true for Si-M distance and M-O distance. In addition, the Si-M and Si-Si distance change significantly, while the M-O distance changes very little with increasing modifier content. The less obvious decreasing trend in the Si-O-M angle and the shorter Si-M distance in magnesium silicate (Fig. 5(c) and (d)) suggest a more rigid connection between SiO₄ tetrahedra and modifier ions.

In Fig. 6, the coordination number of Mg and Ca in magnesium silicate and calcium silicate are in the range of $4.4\sim5$ and $5.3\sim5.9$, respectively, consistent with previous studies [22,56–58]. The coordination number of Mg in magnesium silicate increases with increasing modifier content, whereas the coordination number of Ca in calcium silicate exhibits an increasing trend in the composition range of $10\sim40$ mol% CaO, and then decreases afterwards. The lower coordination number of magnesium manifests its covalent character inside the glass network, which suggests a stronger bond strength between oxygen atom and the modifier.

Fig. 7 shows the primitive ring statistics in magnesium silicate and calcium silicate calculated by using the R.I.N.G.S. program [59]. Here, the primitive rings are defined as the shortest closed loop that includes a given Si atom and two of its nearest neighbor O atoms in the silica



1.624

1.618

1.614

Si-BO (A)

Fig. 3. (a) Q^n species and (b) fraction of different oxygen species as a function of modifier content in magnesium (solid symbol) and calcium (open symbol) silicate glasses at 300 K from classical MD. Error bars are smaller than the symbols. (c) Atomic configuration of $0.5 \text{MgO} - 0.5 \text{SiO}_2$ glass, where the red, blue, and ivory spheres represent the oxygen, silicon, and magnesium atoms, respectively. BO (O bonded to two Si atoms), NBO (O bonded to one Si atom) and FO (O bonded to zero Si atom) are labeled. Red dashed squares highlight one SiO₄ and one MgO₄ tetrahedra.

Fig. 4. Average (a) O-O, (b) Si-BO, and (c) Si-NBO distance as a function of modifier content in magnesium and calcium silicate glasses at 300 K from classical MD. Error bars are smaller than the symbols.

difier content (mol%)

network, only Si and O atoms are considered in calculating the ring statistics [60,61]. In comparison with the ring statistics in silica glass, the ring size distribution shifts toward small-membered rings with increasing modifier content in both magnesium and calcium silicate. The rather high 3-and 4- membered rings in 0.5CaO-0.5SiO₂ glass are attributed to the peak at 60 and 90 degrees in the Si-Si-Si angle distribution, respectively [62] as shown in Fig. 7(d), in comparison with that in magnesium silicate (Fig. 7(c)). Meanwhile, magnesium silicate has more large-sized rings at a given modifier content, and shows less modification to the ring statistics in silica glass at a given modifier content, in a good agreement with the observations in the previous reverse Monte Carlo study [18]. This is consistent with the observations

difier content (mol%)

(a)

2.6

2.63

2.62

0-0 (A)

in Fig. 3 that the addition of modifier leads to more Q^3 species and FOs, but fewer NBOs, thus less disruption to the connectivity of the silica network in magnesium silicate than calcium silicate [63–65].

Modifier content (mol%)

1.612

1.604

Density and elastic moduli from experiments and MD simulations are plotted in Fig. 8. It should be noted, while there are some investigations on calcium silicate glasses in experiments [51,66–73], studies on magnesium silicate glasses are very limited [15], mostly focused on MgO–SiO₂ (MgSiO₃, enstatite) and 2MgO–SiO₂ (Mg₂SiO₄, forsterite) due to their geological importance. Fig. 8 shows that both density and elastic moduli increase with increasing modifier content. At a given modifier content, the density of magnesium silicate is slightly lower than that of calcium silicate except MgO–SiO₂, whereas the elastic moduli of

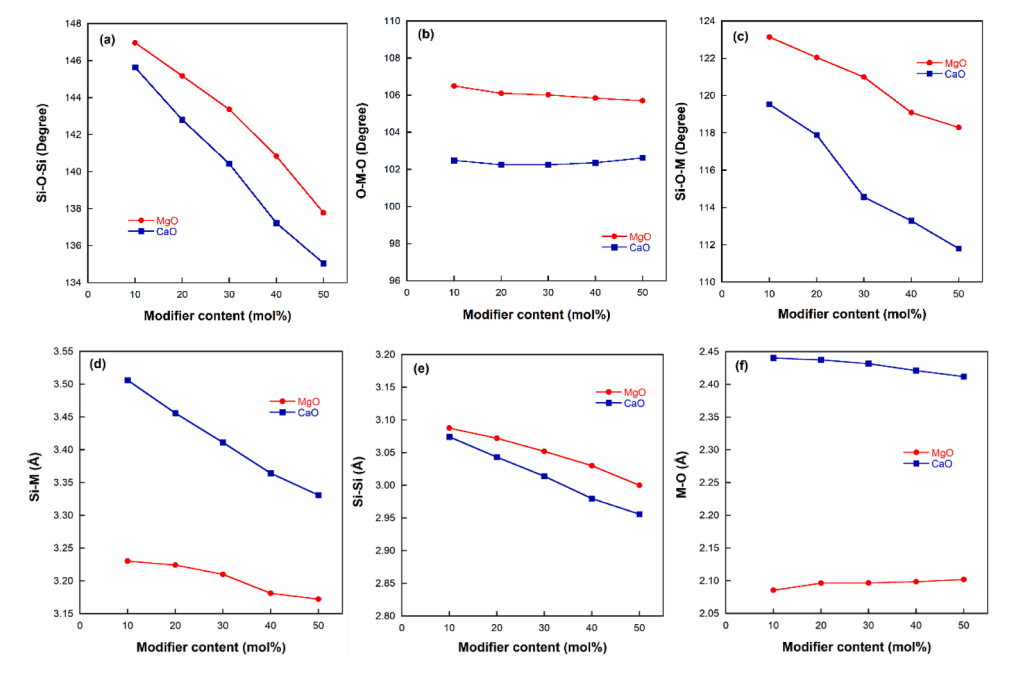


Fig. 5. Average (a) Si-O-Si, (b) O-M-O (M = Mg or Ca), and (c) Si-O-M angle; (d) Si-M, (e) Si-Si, and (f) M-O distance as a function of modifier content in magnesium and calcium silicate glasses at 300 K from classical MD. Error bars are smaller than the symbols.

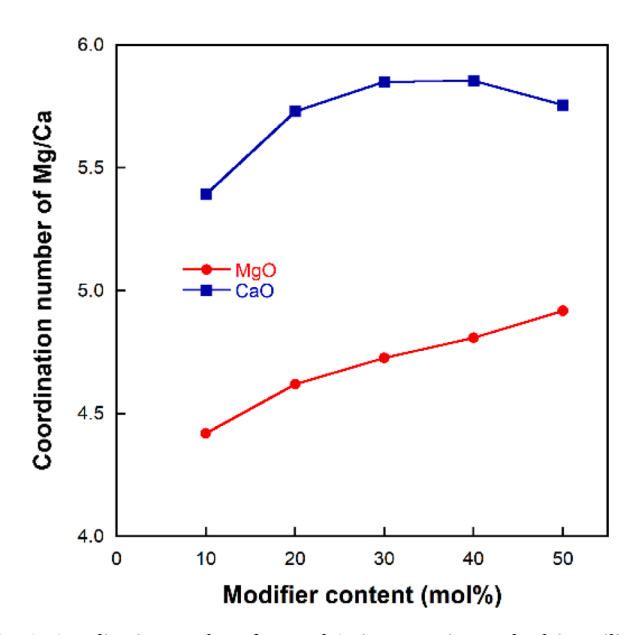


Fig. 6. Coordination number of Mg and Ca in magnesium and calcium silicate glasses as a function of modifier content at 300 K from classical MD.

magnesium silicate are higher than those of calcium silicate in the composition range investigated here. In general, a good agreement is seen between experiments [15,51, 66-73] and MD simulations, although some difference (<10%) in elastic moduli can be seen in Fig. 8 (b) and (c).

In short, the competition between the depolymerization of the glass network and the formation of new bonds between oxygen atoms and modifiers leads to the enhancement of the elastic moduli with increasing modifier content in alkaline earth silicate glasses. The higher elastic moduli of magnesium silicate compared to calcium silicate may result

from the higher connectivity of the overall glass network due to the incorporation of fourfold coordinated magnesium and a more rigid connection between oxygen atoms and modifier ions.

To further validate the reliability of the newly parameterized interaction potential under different thermodynamic conditions, the structure and properties of MgO-SiO₂ (enstatite), CaO-SiO₂ (wollastonite), and 2MgO-SiO2 (forsterite) glasses were investigated and compared with available experimental results [74,75]. The structure factor (S(q)), obtained from the Fourier transform of the total RDF using the R.I.N.G.S. program [59], of vitreous enstatite, wollastonite, and forsterite under different pressures are shown in Fig. 9. Overall, the structure factors from MD simulation well reproduce the experimental neutron structure factors of vitreous enstatite and wollastonite, and X-ray structure factors of vitreous forsterite [74,75]. In all three glasses, the first sharp diffraction peak (FSDP) shifts to a higher q value with increasing pressure. In vitreous enstatite and wollastonite, the intensity of the principal peak around 3 Å^{-1} increases with increasing pressure. For vitreous forsterite, the FSPD sharpens under pressure and an additional peak around 3 Å⁻¹ appears under 20 GPa, which has been associated with the formation of SiO₆ octahedra [76].

Fig. 10 shows that density and elastic moduli of MgO–SiO₂ glass increase with increasing pressure in classical MD simulations, consistent with Brillouin light scattering experiments [70]. The larger difference in density between simulation and experiment in the high pressure region (>10 GPa) may be attributed to the onset of irreversible densification that leads to the underestimated density calculated from sound velocities measured in Brillouin light scattering experiments, which in turn gives lower elastic moduli. This is confirmed by the compression-decompression curve in Fig. 11 (a). The irreversible densification becomes more obvious around 8~10 GPa, corresponding to the pressure at which the population of five-coordinated silicon starts to increase rapidly with pressure as seen in the Fig. 11 (b).

3.3. Structure of magnesium and calcium borate liquids

Fig. 12 shows the partial RDFs of $0.5MgO-0.5B_2O_3$ and $0.5CaO-0.5B_2O_3$ liquids at 3000 K from MD simulations by using the

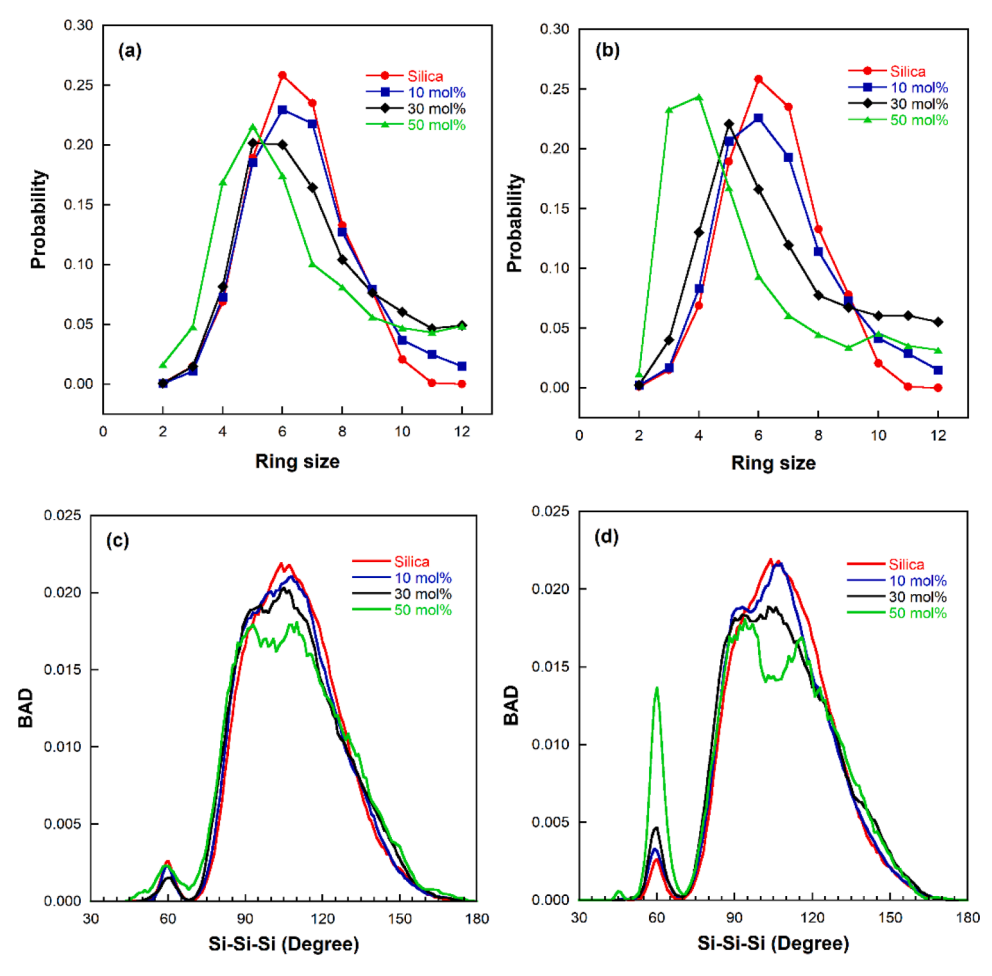


Fig. 7. Ring statistic of (a) magnesium silicate and (b) calcium silicate, Si-Si-Si angle distribution of (c) magnesium silicate and (d) calcium silicate as a function of modifier content at 300 K from classical MD, in comparison with that in silica glass.

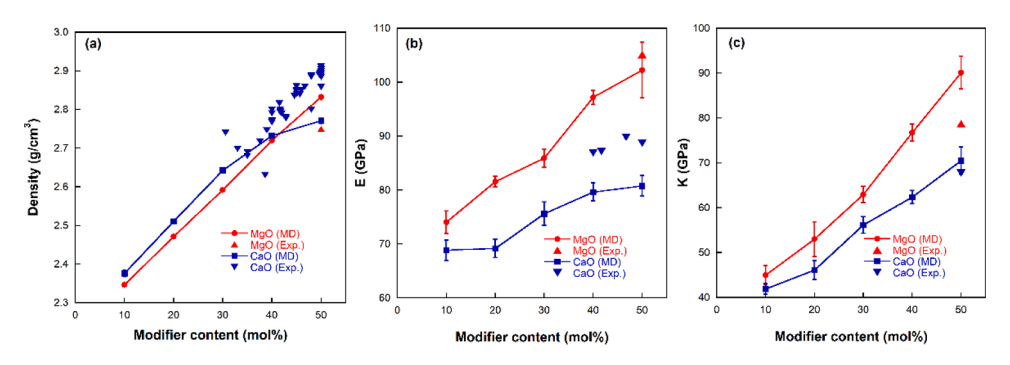


Fig. 8. (a) Density, (b) Young's modulus (*E*), and (c) bulk modulus (*K*) as a function of modifier content in magnesium and calcium silicate glasses at ambient conditions from experiments [15, 51, 66-73] and classical MD.

newly parameterized potential, in a good agreement with $\it ab~initio$ simulation results.

Fig. 13 shows the BADs in $0.5 \text{MgO}-0.5 \text{B}_2 \text{O}_3$ and $0.5 \text{CaO}-0.5 \text{B}_2 \text{O}_3$ liquids at 3000 K by using the newly parameterized potential, overall a good agreement is seen between classical MD and *ab initio* data. The O-M-O bond angle from the classical MD simulation exhibits a more obvious two peaks structure, which may correspond to the splitting of BO-M-BO and NBO-M-NBO bond angle [48,77]. The BAD of B-O-B shifts to the high-angle distribution from classical MD simulation in

comparison to that from *ab initio* simulation, which implies a more open structure in the former than in the latter. The same discrepancy in the BAD of B-O-B was observed in our previous work on alkali borates. As we used the same B-B parameters in the current work, this may be resulted from a deficiency from the previous optimization [32].

3.4. Structure and properties of magnesium and calcium borate glasses

Fig. 14 shows the fraction of fourfold coordinated born (N_4) in

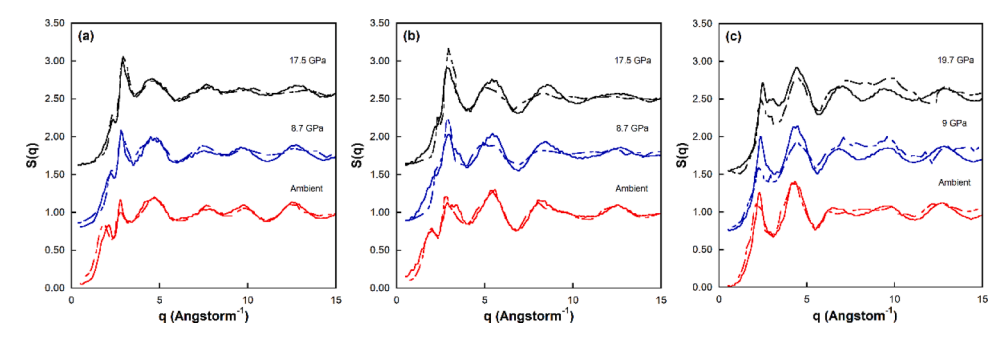


Fig. 9. Neutron structure factor (S(q)) of (a) MgO–SiO₂ (enstatite), (b) CaO–SiO₂ (wollastonite), and X-ray structure factor of (c) 2MgO–SiO₂ (forsterite) glasses under different pressures at room temperature from classical MD (solid line) in comparison with experiments [74, 75] (dashed line). Structure factors at high pressures are shifted vertically for clarity.

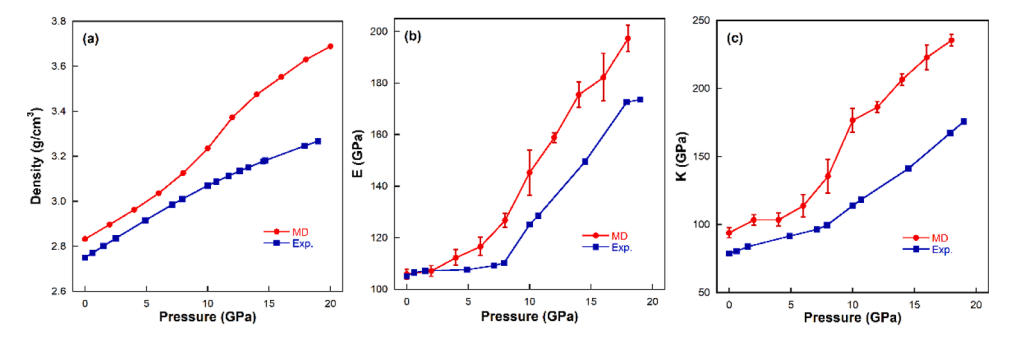


Fig. 10. Variation of (a) density, (b) Young's modulus (*E*), and (c) bulk modulus (*K*) of MgO–SiO₂ glass with pressure at room temperature from classical MD in comparison with experiments [70].

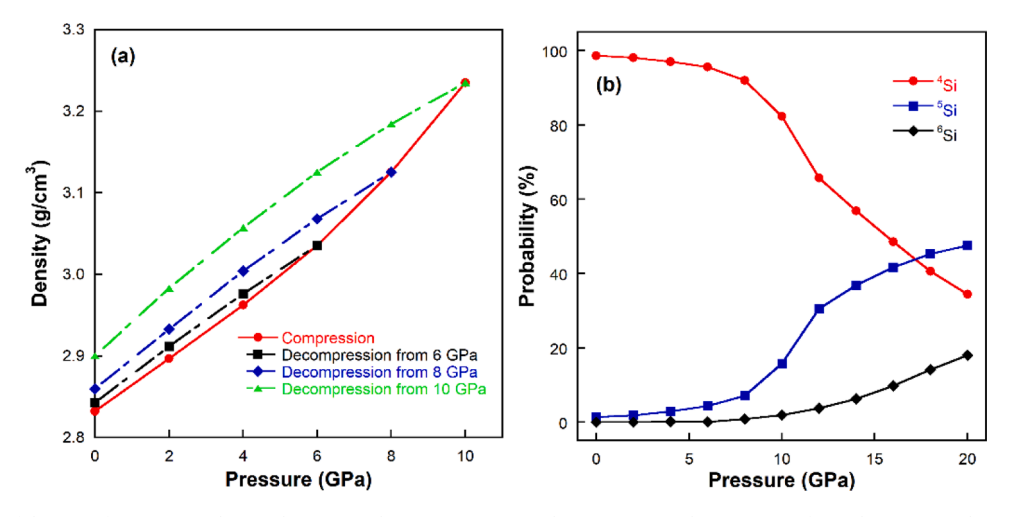


Fig. 11. (a) Variation of density of MgO–SiO₂ glass with pressure during compression-decompression, (b) variation of coordination number of Si of MgO–SiO₂ glass with pressure at 300 K from classical MD.

magnesium and calcium borate glasses. A good agreement is seen between simulations and experiments in the composition range studied [24]. Moreover, the difference in the N_4 values between calcium borate and magnesium borate is well reproduced by the newly parameterized potential. In the narrow composition range studied in experiments, the N_4 changes very little in magnesium borate, with values close to what was predicted in classical MD simulation at 50 mol% of MgO content.

Fig. 15 shows the Q^n species and fraction of different oxygen species in magnesium borate (solid symbol) and calcium borate (open symbol). Overall, magnesium borate shows a slightly larger fraction of boron in

most of the Q^n species, while the Q^4 of BO_4 in calcium borate is much higher than that in magnesium borate. The fraction of different oxygen species in Fig. 15(c) indicates the formation of more NBOs and FOs in magnesium borate compared to calcium borate.

The B-O bond length in BO $_3$ (B^{III}-O) and BO $_4$ (B^{IV}-O) units in magnesium borate and calcium borate are shown in Fig. 16. Overall, the B^{III}-O bond length is shorter than that of the B^{IV}-O bond, which is in good agreement with the experimental data [78]. At a given modifier content, calcium borate exhibits a shorter bond length in both B^{III}-O and B^{IV}-O. Moreover, the bond length of B^{III}-O and B^{IV}-O decrease with increasing

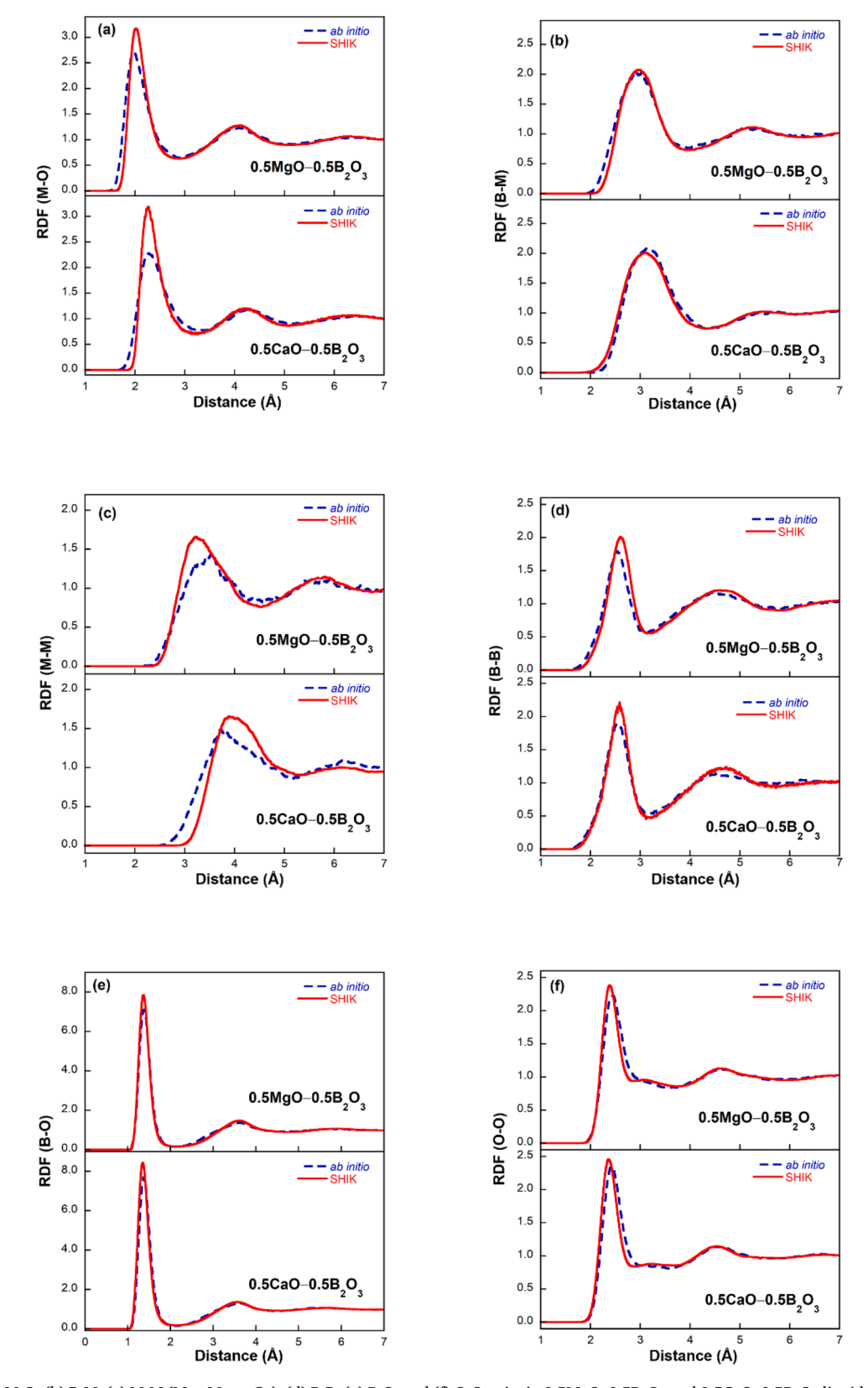


Fig. 12. RDFs of (a) M-O, (b) B-M, (c) M-M (M = Mg or Ca), (d) B-B, (e) B-O, and (f) O-O pairs in $0.5MgO-0.5B_2O_3$ and $0.5CaO-0.5B_2O_3$ liquids obtained from the *ab initio* (blue dashed line) and the SHIK potential (red solid line) simulations at 3000 K.

modifier content and exhibit a less obvious change especially in B^{III}-O units in magnesium borate. The coordination number of Mg and Ca in magnesium borate and calcium borate as a function of modifier content are shown in Fig. 17, which are higher than those in silicates in Fig. 6.

Within the composition range of $10{\sim}50$ mol% modifier content, the coordination number of Mg and Ca exhibits an insignificant change with increasing modifier content.

The higher NBOs and FOs fraction (Fig. 15 (c)) and the lower

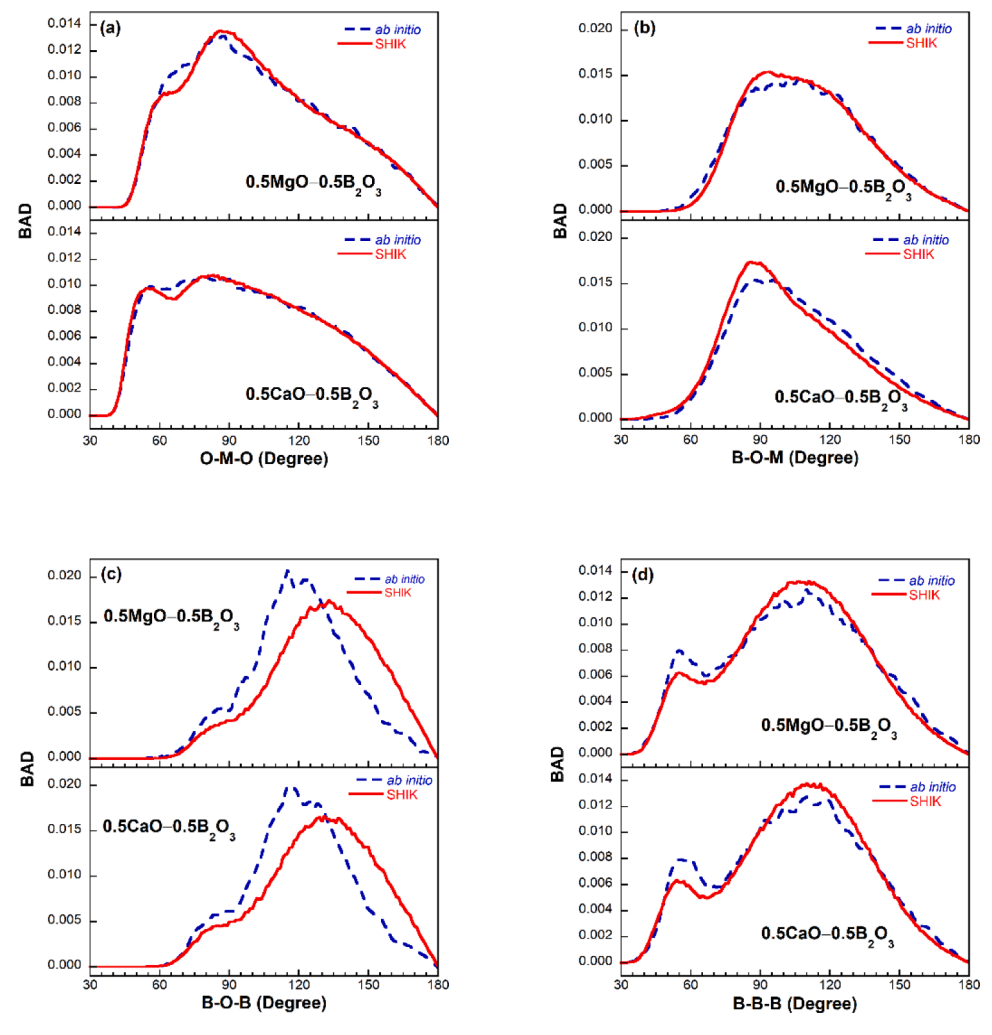


Fig. 13. (a) O-M-O, (b) B-O-M (M=Mg or Ca), (c) B-O-B, and (d) B-B-B BADs in $0.5MgO-0.5B_2O_3$ and $0.5CaO-0.5B_2O_3$ liquids obtained from the *ab initio* (blue dashed line) and the SHIK potential (red solid line) simulations at 3000 K.

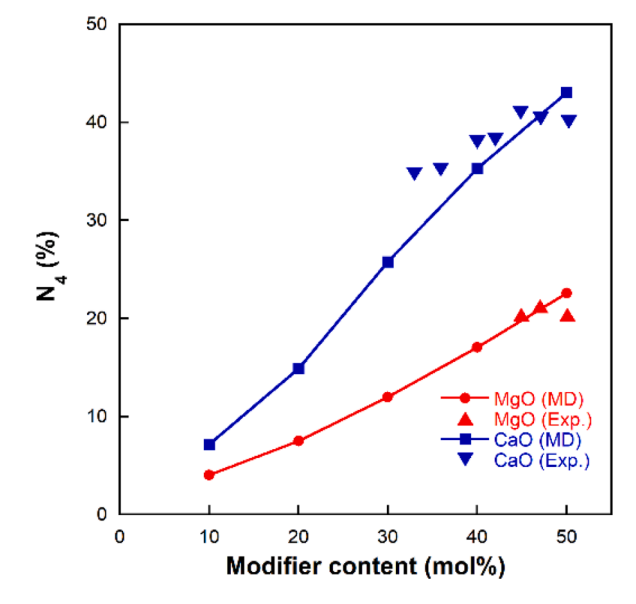


Fig. 14. Fraction of fourfold coordinated boron (N_4) as a function of modifier content in magnesium and calcium borate glasses at ambient conditions from classical MD simulations and experiments [24].

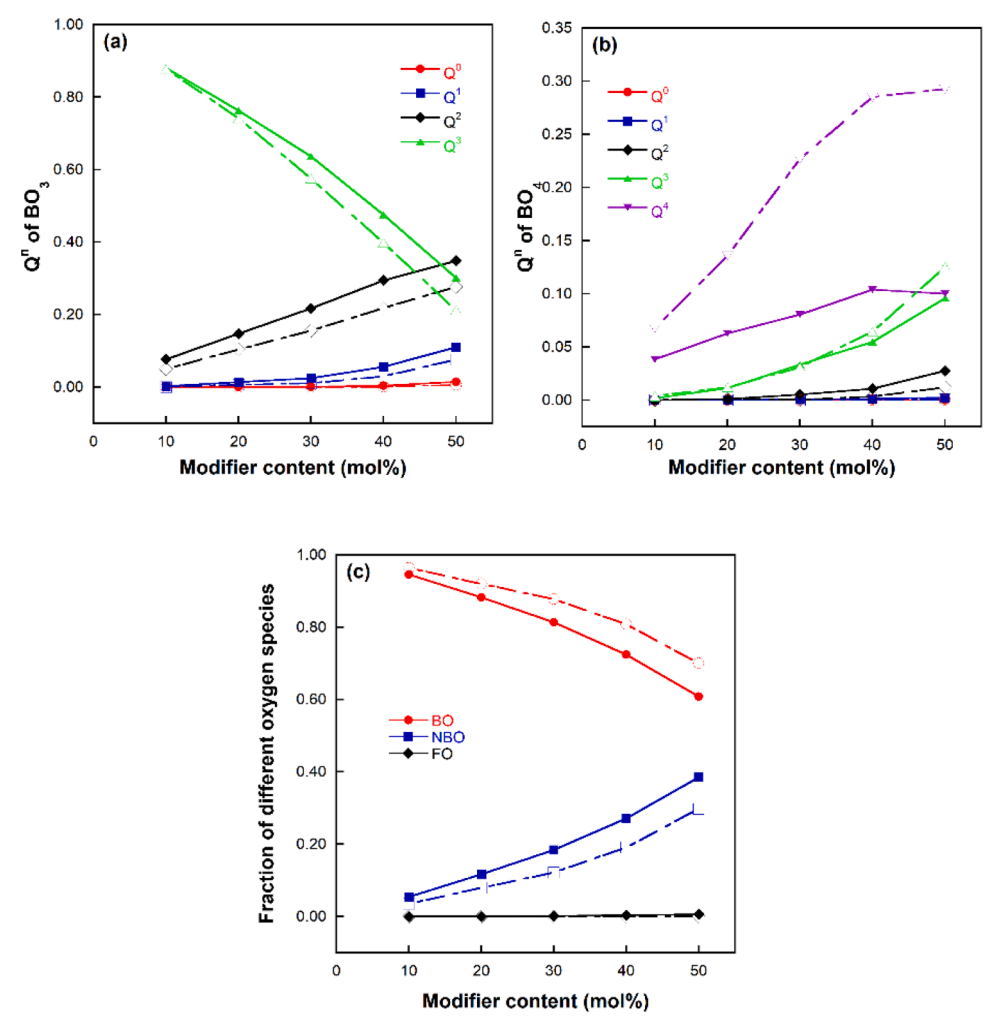


Fig. 15. Q^n species in (a) BO_3 and (b) BO_4 units, and (c) fraction of different oxygen species as a function of modifier content in magnesium (solid symbol) and calcium (open symbol) borate glasses at 300 K from classical MD.

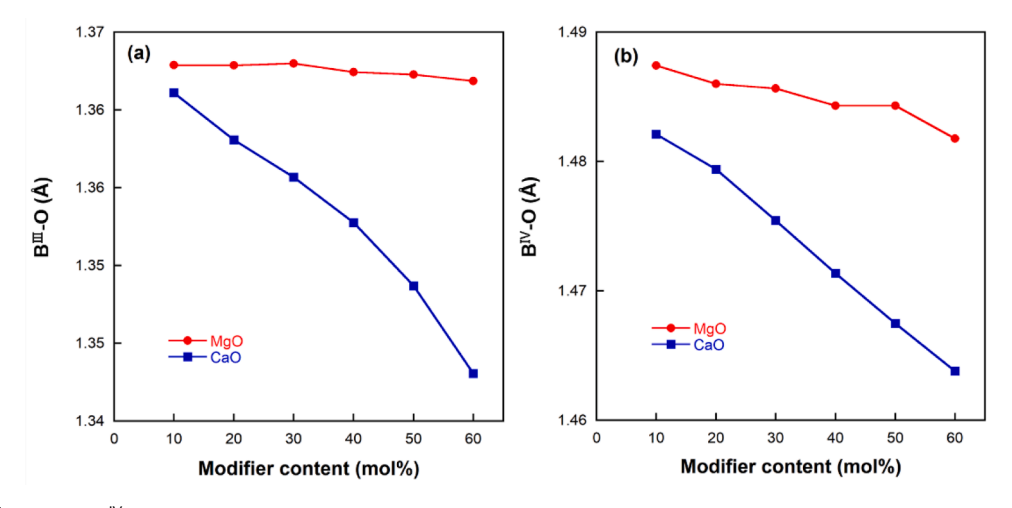


Fig. 16. (a) B^{III}-O and (b) B^{IV}-O bond length as a function of modifier content in magnesium and calcium borate glasses at 300 K from classical MD.

coordination number of modifier (Fig. 17) in magnesium borate suggest that the magnesium may enter the B_2O_3 network instead of converting BO_3 to BO_4 , thus leading to much lower N_4 (Fig. 14) and Q^4 in BO_4 (Fig. 15 (b)) comparing to those in calcium borate with similar modifier contents. This is further verified from the insignificant decrease of the B-O distance with modifier content in magnesium borate, which may be

attributed to the lower conversion rate of BO₃ to BO₄ units (Fig. 16).

Fig. 18 shows that density and elastic moduli of magnesium and calcium borate glasses increase with increasing modifier content, in a good agreement with experimental results [52–55,79–82], except that no experimental value of Young's modulus and bulk modulus are available for magnesium borate to be compared with our simulation

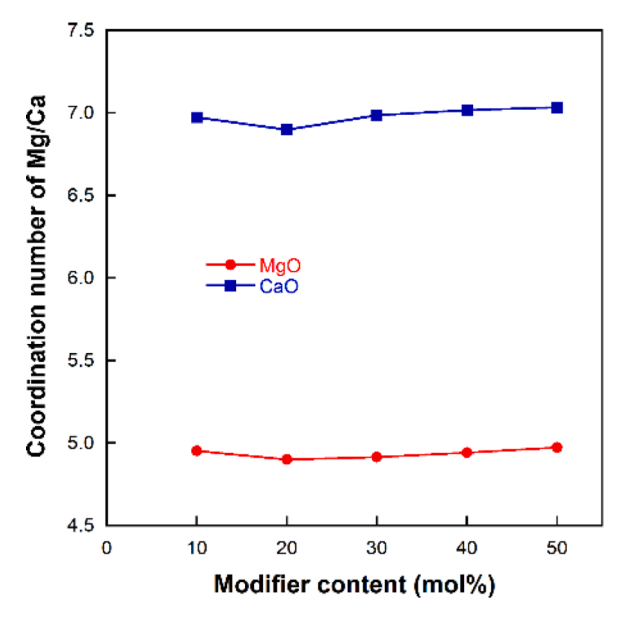


Fig. 17. Coordination number of Mg and Ca in magnesium and calcium borate glasses as a function of modifier content at 300 K from classical MD.

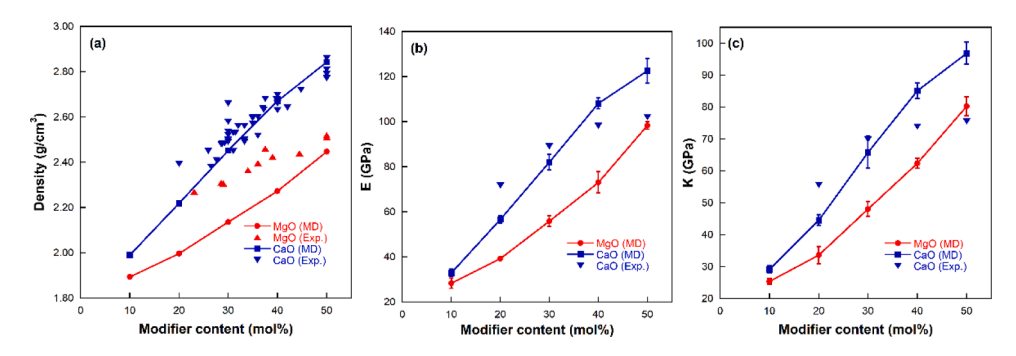


Fig. 18. (a) Density, (b) Young's modulus (*E*), and (c) bulk modulus (*K*) as a function of modifier content in magnesium and calcium borate glasses from MD simulations at ambient conditions in comparison with experiments [52-55, 79-82].

results.

Density and elastic moduli of magnesium borate are lower than those of calcium borate at a given modifier content. In contrast to alkaline earth silicates, the effect of modifier on the elastic moduli of alkaline earth borates is dominated by the formation of fourfold coordinated boron (N_4). The larger amount of N_4 (see Fig. 14) and the shorter B^{III}-O and B^{IV}-O bond length (see Fig. 16) in calcium borate result in a more rigid network structure, thus higher elastic moduli as seen in Fig. 18(b)-(c).

It should be pointed out that phase separation can occur easily in alkaline earth borates due to the limited cooling rates accessible in experiments [52]. No phase separation was observed in our MD simulations due to the orders of magnitude faster quenching rate used. There might be discrepancy in the homogeneity of experimental and simulated samples, which needs to be kept in mind when comparing results from experiments and simulations. Future studies of structure and elastic properties of magnesium borate over a lager composition range are needed to verify the predictions from our MD simulations and to fine tune the potential if necessary.

4. Conclusions

Pairwise interatomic potentials for alkaline earth silicate and borate were newly parameterized and used to study the structure and properties of magnesium silicate and borate over a large composition range and

compared with those of calcium silicate and borate. The competition between the depolymerization of the glass network and the formation of new bonds between oxygen atoms and the modifiers leads to the enhancement of the elastic moduli with increasing modifier content in alkaline earth silicate glasses. The higher elastic moduli in magnesium silicate may result from the higher connectivity of the over glass network due to the incorporation of fourfold coordinated magnesium and a more rigid connection between oxygen atoms and modifier ions. In contrast to the silicates, the effect of modifier on the elastic moduli of alkaline earth borates is dominated by the formation of fourfold coordinated boron (N_4). Calcium borate with higher N_4 shows a more rigid network structure and higher elastic moduli.

Data availability

The data that support the findings of this study are available from the corresponding author upon reasonable request. Potential files to be compiled with the LAMMPS source code and example input scripts for LAMMPS can be accessed at: https://github.com/compmatscirpi/SHIK-potential.

CRediT authorship contribution statement

Yueh-Ting Shih: Investigation, Formal analysis, Writing - original draft, Writing - review & editing. Siddharth Sundararaman:

Investigation, Formal analysis, Writing - review & editing. **Simona Ispas:** Conceptualization, Writing - review & editing. **Liping Huang:** Supervision, Funding acquisition, Conceptualization, Writing - review & editing.

Declaration of Competing Interest

The authors declare that they have no known competing financial interests or personal relationships that could have appeared to influence the work reported in this paper.

Acknowledgments

This work was supported by the National Science Foundation under grant no. DMR-1508410 and DMR-1936368. We thank Dr. Walter Kob at the University of Montpellier for his contribution to the development of the earlier version of the SHIK potential and for his continued support for this work.

References

- [1] S. Kokubo, R. Fujimoto, S. Yokota, S. Fukushima, K. Nozaki, K. Takahashi, K. Miyata, Bone regeneration by recombinant human bone morphogenetic protein-2 and a novel biodegradable carrier in a rabbit ulnar defect model, Biomaterials 24 (2003) 1643–1651.
- [2] P. Saravanapavan, L.L. Hench, Mesoporous calcium silicate glasses. I. Synthesis, J. Non Cryst. Solids 318 (2003) 1–13.
- [3] R.J.M. Pellenq, A. Kushima, R. Shahsavari, K.J. Van Vliet, M.J. Buehler, S. Yip, F.-J. Ulm, A realistic molecular model of cement hydrates, Proc. Natl. Acad. Sci. 106 (2009) 16102.
- [4] H. Ma, Z. Li, Realistic pore structure of portland cement paste: experimental study and numerical simulation, Comput. Concrete 11 (2013) 317–336.
- [5] D. Hou, T. Zhao, Z. Jin, H. Ma, Z. Li, Molecular simulation of calcium silicate composites: structure, dynamics, and mechanical properties, J. Am. Ceram. Soc. 98 (2015) 758–769.
- [6] M. Vallet-Regí, Ceramics for medical applications, J. Chem. Soc.-Dalton Trans. 2 (2001) 97–108.
- [7] F. Barrere, C.A. van Blitterswijk, K. de Groot, P. Layrolle, Influence of ionic strength and carbonate on the Ca-P coating formation from SBF×5 solution, Biomaterials 23 (2002) 1921–1930.
- [8] A. Pedone, G. Malavasi, M.C. Menziani, Computational insight into the effect of CaO/MgO substitution on the structural properties of phospho-silicate bioactive glasses, J. Phys. Chem. C 113 (2009) 15723–15730.
- [9] S.J. Watts, R.G. Hill, M.D. O'Donnell, R.V. Law, Influence of magnesia on the structure and properties of bioactive glasses, J. Non Cryst. Solids 356 (2010) 517, 524
- [10] A. Pedone, G. Malavasi, M.C. Menziani, U. Segre, A.N. Cormack, Role of magnesium in soda-lime glasses: insight into structural, transport, and mechanical properties through computer simulations, J. Phys. Chem. C 112 (2008) 11034-11041
- [11] A.K. Varshneya, J.C. Mauro, Chapter 5 glass compositions and structures, in: A. K. Varshneya, J.C. Mauro (Eds.), Fundamentals of Inorganic Glasses (Third Edition), Elsevier, 2019, pp. 101–164.
- [12] G. Hauret, Y. Vaills, Y. Luspin, F. Gervais, B. Coté, Similarities in the behaviour of magnesium and calcium in silicate glasses, J. Non Cryst. Solids 170 (1994) 175–181.
- [13] S. Kohara, K. Suzuya, K. Takeuchi, C.K. Loong, M. Grimsditch, J.K.R. Weber, J. A. Tangeman, T.S. Key, Glass formation at the limit of insufficient network formers, Science 303 (2004) 1649.
- [14] D.R. Neuville, L. Cormier, V.r. Montouillout, P. Florian, F. Millot, J.-C. Rifflet, D. Massiot, Amorphous materials: properties, structure, and durability: Structure of Mg- and Mg/Ca aluminosilicate glasses: ²⁷Al NMR and Raman spectroscopy investigations, Am. Mineral. 93 (2008) 1721–1731.
- [15] S. Sen, J. Tangeman, Evidence for anomalously large degree of polymerization in Mg2SiO4 glass and melt, Am. Mineral. 93 (2008) 946–949.
- [16] R.G. Kuryaeva, The state of magnesium in silicate glasses and melts, Glass Phys. Chem 35 (2009) 378–383.
- [17] L. Cormier, G. Calas, G.J. Cuello, Structural study of Ca–Mg and K–Mg mixing in silicate glasses by neutron diffraction, J. Non Cryst. Solids 356 (2010) 2327–2331.
- [18] L. Cormier, G.J. Cuello, Structural investigation of glasses along the MgSiO₃-CaSiO₃ join: diffraction studies, Geochim. Cosmochim. Acta 122 (2013) 498–510.
- [19] B.M. Al-Hasni, G. Mountjoy, A molecular dynamics study of the atomic structure of x(MgO) 100-x(SiO₂), J. Non Cryst. Solids 400 (2014) 33–44.
- [20] X. Bidault, S. Chaussedent, W. Blanc, A simple transferable adaptive potential to study phase separation in large-scale xMgO-(1-x)SiO₂ binary glasses, J. Chem. Phys. 143 (2015), 154501.
- [21] C. Calahoo, J.W. Zwanziger, The mixed modifier effect in ionic conductivity and mechanical properties for xMgO-(50-x)CaO-50SiO₂ glasses, J. Non Cryst. Solids 460 (2017) 6–18.

- [22] M.C. Wilding, C.J. Benmore, J.A. Tangeman, S. Sampath, Coordination changes in magnesium silicate glasses, Europhys. Lett. (EPL) 67 (2004) 212–218.
- [23] W.J. Dell, P.J. Bray, The Determination of phase-relations in the system MgO-B₂O₃ at the metaborate compostion using B-11 NMR, Phys. Chem. Glasses 23 (1982) 98-100
- [24] Y.D. Yiannopoulos, G.D. Chryssikos, E.I. Kamitsos, Structure and properties of alkaline earth borate glasses, Phys. Chem. Glasses 42 (2001) 164–172.
- [25] M. Wang, N.M. Anoop Krishnan, B. Wang, M.M. Smedskjaer, J.C. Mauro, M. Bauchy, A new transferable interatomic potential for molecular dynamics simulations of borosilicate glasses, J. Non Cryst. Solids 498 (2018) 294–304.
- [26] L. Deng, J. Du, Development of boron oxide potentials for computer simulations of multicomponent oxide glasses, J. Am. Ceram. Soc. 102 (2019) 2482–2505.
- [27] B. Guillot, N. Sator, A computer simulation study of natural silicate melts. Part I: low pressure properties, Geochim. Cosmochim. Acta 71 (2007) 1249–1265.
- [28] L.-H. Kieu, J.M. Delaye, L. Cormier, C. Stolz, Development of empirical potentials for sodium borosilicate glass systems, J. Non Cryst. Solids 357 (2011) 3313–3321.
- [29] K.-H. Lee, Y. Yang, B. Ziebarth, W. Mannstadt, M.J. Davis, J.C. Mauro, Evaluation of classical interatomic potentials for molecular dynamics simulations of borosilicate glasses, J. Non Cryst. Solids 528 (2020), 119736.
- [30] S. Sundararaman, L. Huang, S. Ispas, W. Kob, New optimization scheme to obtain interaction potentials for oxide glasses, J. Chem. Phys. 148 (2018), 194504.
- [31] S. Sundararaman, L. Huang, S. Ispas, W. Kob, New interaction potentials for alkali and alkaline-earth aluminosilicate glasses, J. Chem. Phys. 150 (2019), 154505.
- [32] S. Sundararaman, L. Huang, S. Ispas, W. Kob, New interaction potentials for borate glasses with mixed network formers, J. Chem. Phys. 152 (2020), 104501.
- [33] R.A. Buckingham, J.E. Lennard-Jones, The classical equation of state of gaseous helium, neon and argon, Proc. R. Soc. Lond. Ser. A. Math. Phys. Sci. 168 (1938) 264–283.
- [34] D. Wolf, P. Keblinski, S.R. Phillpot, J. Eggebrecht, Exact method for the simulation of Coulombic systems by spherically truncated, pairwise $\rm r^{-1}$ summation, J. Chem. Phys. 110 (1999) 8254–8282.
- [35] A. Carré, L. Berthier, J. Horbach, S. Ispas, W. Kob, Amorphous silica modeled with truncated and screened Coulomb interactions: a molecular dynamics simulation study, J. Chem. Phys. 127 (2007), 114512.
- [36] J. Habasaki, I. Okada, Molecular dynamics simulation of alkali silicates based on the quantum mechanical potential surfaces, Mol. Simul. 9 (1992) 319–326.
- [37] S. Plimpton, Fast parallel algorithms for short-range molecular dynamics, J. Comput. Phys. 117 (1995) 1–19.
- [38] K. Levenberg, A method for the solution of certain non-linear problems in least squares, Q. Appl. Math. 2 (1944) 164–168.
- [39] D.W. Marquardt, An algorithm for least-squares estimation of nonlinear parameters, J. Soc. Ind. Appl. Math. 11 (1963) 431–441.
- [40] G. Kresse, J. Furthmüller, Efficiency of ab-initio total energy calculations for metals and semiconductors using a plane-wave basis set, Comput. Mater. Sci. 6 (1996) 15–50.
- [41] G. Kresse, J. Furthmüller, Efficient iterative schemes for ab initio total-energy calculations using a plane-wave basis set, Phys. Rev. B 54 (1996) 11169–11186.
- [42] J.P. Perdew, K. Burke, M. Ernzerhof, Generalized gradient approximation made simple, Phys. Rev. Lett. 77 (1996) 3865–3868.
- [43] R.M. Martin, R.M. Martin, C.U. Press, Electronic Structure: Basic Theory and Practical Methods, Cambridge University Press, 2004.
- [44] J.P. Perdew, A. Ruzsinszky, G.I. Csonka, O.A. Vydrov, G.E. Scuseria, L. A. Constantin, X. Zhou, K. Burke, Restoring the density-gradient expansion for exchange in solids and surfaces, Phys. Rev. Lett. 100 (2008), 136406.
- [45] P.E. Blöchl, Projector augmented-wave method, Phys. Rev. B 50 (1994) 17953–17979.
- [46] G. Kresse, D. Joubert, From ultrasoft pseudopotentials to the projector augmentedwave method, Phys. Rev. B 59 (1999) 1758–1775.
- [47] L. Pedesseau, S. Ispas, W. Kob, First-principles study of a sodium borosilicate glass-former. I. The liquid state, Phys. Rev. B 91 (2015), 134201.
- [48] L. Pedesseau, S. Ispas, W. Kob, First-principles study of a sodium borosilicate glass-former. II. The glass state, Phys. Rev. B 91 (2015), 134202.
- [49] S. Nosé, A molecular dynamics method for simulations in the canonical ensemble, Mol. Phys. 52 (1984) 255–268.
- [50] A. Pedone, G. Malavasi, M.C. Menziani, A.N. Cormack, U. Segre, A new self-consistent empirical interatomic potential model for oxides, silicates, and silicabased glasses, J. Phys. Chem. B 110 (2006) 11780–11795.
- [51] M. Schwartz, J.D. Mackenzie, Ionic conductivity in calcium silicate glasses, J. Am. Ceram. Soc. 49 (1966) 582–585.
- [52] N.P. Lower, J.L. McRae, H.A. Feller, A.R. Betzen, S. Kapoor, M. Affatigato, S. A. Feller, Physical properties of alkaline-earth and alkali borate glasses prepared over an extended range of compositions, J. Non Cryst. Solids 293-295 (2001) 669-675.
- [53] K.S.Thind Manupriya, G. Sharma, V. Rajendran, K. Singh, A.V. Gayathri Devi, S. Aravindan, Structural and acoustic investigations of calcium borate glasses, Physica Status Solidi(a) 203 (2006) 2356–2364.
- [54] T. Mullenbach, M. Franke, A. Ramm, A.R. Betzen, S. Kapoor, N. Lower, T. Munhollon, M. Berman, M. Affatigato, S.A. Feller, Structural characterisation of alkaline earth borosilicate glasses through density modelling, Phys. Chem. Glasses -Eur. J. Glass Sci. Technol. Part B 50 (2009) 89–94.
- [55] S. Feller, T. Mullenbach, M. Franke, S. Bista, A. O'Donovan-Zavada, K. Hopkins, D. Starkenberg, J. McCoy, D. Leipply, J. Stansberry, E. Troendle, M. Affatigato, D. Holland, M. Smith, S. Kroeker, V. Michaelis, J. Wren, Structure and properties of barium and calcium borosilicate glasses, Phys. Chem. Glasses - Eur. J. Glass Sci. Technol. Part B 53 (2012).

- [56] M.C. Eckersley, P.H. Gaskell, A.C. Barnes, P. Chieux, Structural ordering in a calcium silicate glass, Nature 335 (1988) 525–527.
- [57] M.C. Wilding, C.J. Benmore, J.K.R. Weber, Changes in the local environment surrounding magnesium ions in fragile MgO-SiO₂ liquids, EPL (Europhys. Lett.) 89 (2010) 26005.
- [58] L. Cormier, G.J. Cuello, Mg coordination in a MgSiO₃ glass using neutron diffraction coupled with isotopic substitution, Phys. Rev. B 83 (2011), 224204.
- [59] S.Le Roux, P. Jund, Ring statistics analysis of topological networks: new approach and application to amorphous GeS₂ and SiO₂ systems, Comput. Mater. Sci. 49 (2010) 70–83.
- [60] K. Goetzke, H.J. Klein, Properties and efficient algorithmic determination of different casses of rings in finite and infinite polyhedral networks, J. Non Cryst. Solids 127 (1991) 215–220.
- [61] X. Yuan, A.N. Cormack, Efficient algorithm for primitive ring statistics in topological networks, Comput. Mater. Sci. 24 (2002) 343–360.
- [62] J.P. Rino, I. Ebbsjo, R.K. Kalia, A. Nakano, P. Vashishta, Structure of rings in vitreous SiO₂, Phys. Rev. B 47 (1993) 3053–3062.
- [63] P. Zhang, P.J. Grandinetti, J.F. Stebbins, Anionic species determination in CaSiO₃ glass using two-dimensional ²⁹Si NMR, J. Phys. Chem. B 101 (1997) 4004–4008.
- [64] N.K. Nasikas, T.G. Edwards, S. Sen, G.N. Papatheodorou, Structural characteristics of novel Ca–Mg orthosilicate and suborthosilicate glasses: results from ²⁹Si and ¹⁷O NMR spectroscopy, J. Phys. Chem. B 116 (2012) 2696–2702.
- [65] L.M. Thompson, R.J. McCarty, J.F. Stebbins, Estimating accuracy of ¹⁷O NMR measurements in oxide glasses: constraints and evidence from crystalline and glassy calcium and barium silicates, J. Non Cryst. Solids 358 (2012) 2999–3006.
- [66] N. Iwamoto, Y. Makino, S. Kasahara, Correlation between refraction basicity and theoretical optical basicity Part I. Alkaline and alkaline-earth silicate glasses, J. Non Cryst. Solids 68 (1984) 379–388.
- [67] C. Huang, E.C. Behrman, Structure and properties of calcium aluminosilicate glasses, J. Non Cryst. Solids 128 (1991) 310–321.
- [68] S. Inaba, S. Fujino, K. Morinaga, Young's Modulus and compositional parameters of oxide glasses, J. Am. Ceram. Soc. 82 (1999) 3501–3507.
- [69] F.V. Natrup, H. Bracht, S. Murugavel, B. Roling, Cation diffusion and ionic conductivity in soda-lime silicate glasses, PCCP 7 (2005) 2279–2286.
- [70] C. Sanchez-Valle, J.D. Bass, Elasticity and pressure-induced structural changes in vitreous MgSiO₃-enstatite to lower mantle pressures, Earth Planet. Sci. Lett. 295 (2010) 523–530.

- [71] D.C. Kaseman, A. Retsinas, A.G. Kalampounias, G.N. Papatheodorou, S. Sen, Q-speciation and network structure evolution in invert calcium silicate glasses, J. Phys. Chem. B 119 (2015) 8440–8445.
- [72] C.C. Lin, K.S. Leung, P. Shen, S.F. Chen, Elasticity and structure of the compounds in the wollastonite (CaSiO₃)-Na₂SiO₃ system: from amorphous to crystalline state, J. Mater. Sci. Mater. Med. 26 (2015) 5361.
- [73] S. Takahashi, D.R. Neuville, H. Takebe, Thermal properties, density and structure of percalcic and peraluminus CaO–Al₂O₃–SiO₂ glasses, J. Non Cryst. Solids 411 (2015) 5–12.
- [74] C.J. Benmore, E. Soignard, M. Guthrie, S.A. Amin, J.K.R. Weber, K. McKiernan, M. C. Wilding, J.L. Yarger, High pressure x-ray diffraction measurements on Mg₂SiO₄ glass, J. Non Cryst. Solids 357 (2011) 2632–2636.
- [75] P.S. Salmon, G.S. Moody, Y. Ishii, K.J. Pizzey, A. Polidori, M. Salanne, A. Zeidler, M. Buscemi, H.E. Fischer, C.L. Bull, S. Klotz, R. Weber, C.J. Benmore, S. G. MacLeod, Pressure induced structural transformations in amorphous MgSiO₃ and CaSiO₃, J. Non-Cryst. Solids: X 3 (2019), 100024.
- [76] C. Meade, R.J. Hemley, H.K. Mao, High-pressure x-ray diffraction of SiO₂ glass, Phys. Rev. Lett. 69 (1992) 1387–1390.
- [77] A. Tilocca, Sodium migration pathways in multicomponent silicate glasses: car–parrinello molecular dynamics simulations, J. Chem. Phys. 133 (2010), 014701.
- [78] R.L. Mozzi, B.E. Warren, The structure of vitreous boron oxide, J. Appl. Crystallogr. 3 (1970) 251–257.
- [79] L. Shartsis, H.F. Shermer, Surface tension, density, viscosity, and electrical resistivity of molten binary alkaline-earth borates, J. Am. Ceram. Soc. 37 (1954) 544-551
- [80] H. Singh, K. Singh, G. Sharma, L. Gerward, R. Nathuram, B.S. Lark, H.S. Sahota, A. Khanna, Barium and calcium borate glasses as shielding materials for x-rays and gamma-rays, Phys. Chem. Glasses - Eur. J. Glass Sci. Technol. Part B 44 (2003) 5–8.
- [81] L. Donohoe, J. Shelbyy, Formation and properties of soda-lime borate glasses, Phys. Chem. Glasses - Eur. J. Glass Sci. Technol. Part B 47 (2006) 16–21.
- [82] S. Sanghi, S. Rani, A. Agarwal, V. Bhatnagar, Influence of Nb₂O₅ on the structure, optical and electrical properties of alkaline borate glasses, Mater. Chem. Phys. 120 (2010) 381–386.